ISTITUTO NAZIONALE DI FISICA NUCLEARE

Sezione di Trieste

INFN/AE-92/17

26 maggio 1992

G. Barbiellini, G. Basini, V. Bidoli, M. Bocciolini, M. Boezio, F. Bongiorno, F. Massimo Brancaccio, M.T. Brunetti, A. Buccheri, M. Candusso, F. Celletti, A. Codino, C. De Fabritiis, M.P. De Pascale, F. Fratnik, A. Incicchitti, M. Menichelli, M. Miozza, A. Morselli, A. Perego, P. Picozza, D. Prosperi, I. Salvadori, P. Schiavon, P. Spillantini, M. Ricci, A. Vacchi and N. Zampa

A SILICON IMAGING CALORIMETER PROTOTYPE FOR ANTIMATTER SEARCH IN SPACE: EXPERIMENTAL RESULTS

Servizio Documentazione
dei Laboratori Nazionali di Frascati

A SILICON IMAGING CALORIMETER PROTOTYPE FOR ANTIMATTER SEARCH IN SPACE: EXPERIMENTAL RESULTS

M. Bocciolini, F. Celletti, A. Perego, P. Spillantini
Dipartimento di Fisica dell'Università di Firenze, Italy
and
Sezione INFN di Firenze

G. Basini, F. Bongiorno*), F. Massimo Brancaccio, M. Ricci
Laboratori Nazionali di Frascati dell'INFN, Frascati

M.T. Brunetti, A.Codino, M. Menichelli, M.Miozza, I. Salvatori
Dipartimento di Fisica dell'Università di Perugia, Italy
and
Sezione INFN di Perugia

V. Bidoli, M. Candusso, C. De Fabritiis, M.P. De Pascale, A. Morselli, P. Picozza
Dipartimento di Fisica dell'Università "Tor Vergata", Roma, Italy
and
Sezione INFN di Roma II

A. Buccheri, A. Incicchitti, D. Prosperi
Dipartimento di Fisica dell'Università "La Sapienza", Roma, Italy
and
Sezione INFN di Roma

G. Barbiellini, M. Boezio, F. Fratnik, P. Schiavon, A. Vacchi, N. Zampa
Dipartimento di Fisica dell'Università di Trieste, Italy
and
Sezione INFN di Trieste

Submitted to Nuclear Instruments and Methods in Physics Research

---

*) Also at Dipartimento di Metodi e Modelli Matematici dell'Università `La Sapienza', Roma, Italy

ABSTRACT

This report presents the results obtained with a prototype silicon–tungsten (Si–W), electromagnetic calorimeter conceived as a fine-grained imaging device to carry out studies of the antimatter component in primary cosmic radiation.

The calorimeter prototype contains 20 *xy* sampling layers interleaved with 19 showering material planes. One sensitive layer is obtained with two silicon strip detectors (Si-D) (60×60) mm^2, each divided into 16 strips, 3.6 mm wide; the two detectors are assembled back to back with perpendicular strips. This allows the transverse distributions of the shower in both coordinates at each sampling (0.5 X_0) to be pictured. The basic characteristics of the design and the experimental results obtained on a test beam at the CERN Proton Synchrotron (PS) for electrons and pions are reported. The main results presented are the response of the calorimeter to the electron at various energies (1–8 GeV), and the transverse shower profiles at different calorimeter depths as well as the patterns of the electromagnetic shower and those of the interacting and non-interacting pions. The capability of the calorimeter in measuring the direction of the incoming electromagnetic particle from the pattern of the shower has been evaluated at different energies. These results are encouraging in view of the possible use of this detector to search for high-energy γ sources in space.

1. INTRODUCTION

The detector is a prototype of the electromagnetic calorimeter conceived for the WiZard [1] experiment to investigate, in a planned space mission, the antimatter component in primary cosmic radiation. Beside the calorimeter, the WiZard apparatus is composed of a momentum-analyser superconducting magnet with drift-chamber tracking, a transition radiation detector, and a time-of-flight system.

Minimum ionizing particles (mip) produce about 80 electron–hole pairs per μm of Si-D crossed; the corresponding charge collection is a process not subject to instabilities or non-linear effects. The segmentation of each Si-D provides the calorimeter with a high spatial granularity. The shower profile is measured at each sampling plane in both the x and y coordinates.

The allowed weight for the mentioned space applications limits the calorimeter depth to about 10 X_0, which is insufficient for the full energy containment of high-energy electromagnetic particles. The good granularity and energy resolution of the silicon detectors makes them capable of measuring the transverse and longitudinal shower profiles and the tracks of the particles with high accuracy [2], thus allowing good particle identification also in the absence of the full shower containment.

Experimental data from calorimeters based on silicon as an active material have already been published [3] - [7]. In the present paper more evidence is given about the results concerning high segmentation and shower-imaging capability; beside its characteristics as a particle identifier, the calorimeter achieves good accuracy (a few mrad) in reconstructing the direction of the incoming particle. The use of a large-area Si-D greatly facilitates the construction of large sensitive surfaces; this prototype calorimeter is the first constructed with detectors having an area of (60×60) mm^2. The detectors are kept in a special package which, when patched together to form large surfaces, allow a minimal dead area for the sampling planes of the calorimeter.

The Si–W calorimeter can play a decisive role in the event definition, especially in the search for antimatter in cosmic radiation. Moreover, the data from the first few planes of this calorimeter can be considered as a source of information for the design of a pre-shower detector.

2. THE TRACKING CALORIMETER

The calorimeter prototype, whose characteristics are reported in the table 1, consists of 20 layers of silicon detectors*) alternated with 19 planes of tungsten. The thickness of the material crossed by the incident beam before the first sensitive layer corresponds to 0.2 X_0.

Table 1

Si–W prototype calorimeter characteristics

Active area	59×59 mm ^{2}
Number of Si-D x, y sampling	20
Number of tungsten plates	19
Thickness of the Si-D per sampling	2×380 μm
Thickness of the tungsten plates	1.75 mm (0.5 X_0)
Total depth (W)	9.5 X_0
Pitch of the strips on the Si-D	3.6 mm
Distance between sampling layers	24.5 mm
Working voltage (>full depletion)	80 V
Number of electronic channels	640
Power dissipation per channel	15 mW

In the design of this prototype we were bound by the constraints, common to all experiments in space, of limited weight, low power consumption, and high reliability. In addition, structural constraints affect the geometrical parameter of the calorimeter and, in particular, the distance between the sensitive planes. The transverse granularity was chosen for the aims of the WiZard apparatus through Monte Carlo calculations (MC) [2] . One sensitive element is composed of two Si detectors mounted back to back with an on-line pin structure and perpendicular strips to give x and y coordinates as shown in fig.1, for the Si-D this allows the use of a well-established technology suitable for highly automatized mass production and low costs. The dead area, due to the wire bonding to the ceramic support, is less than 2%.

---

*) Built at Camberra (Belgium), Hamamatsu (Japan), and SGS (Italy)

The general characteristics of one Si-D are listed in table 2.

Table 2
Si-D characteristics

Total area	(60×60) mm^2
Number of strips	16
Thickness	(380 ± 15) μm
Strip pitch	3.6 mm
Crystal	n-type, (FZ) Si, $R \geq 4$ kΩ cm
Read–out coupling	ohmic
Strip capacitance	≈ 70 pF

All the Si-D's used in this prototype are analysed before, during, and after the packaging procedure, and the parameters of each strip are stored in a data base available for studies of radiation resistance and long-term stability. Figure 2 shows the results from typical measurements of the dark current and capacity of the strip plotted against the bias voltage. Each detector assembly is mounted on a multilayer board, which also carries the front-end electronics and the related wiring. The calorimeter prototype is contained in an aluminium box which has one of its side walls made of a multilayer board to provide the connections of the detector's card to the outside electronics (see fig. 3).

The design of the readout electronics [8] has been specifically developed to take into account the future application of the calorimeter in space research. It has been conceived for low-power consumption (15 mW/per channel) and low electronic noise, i.e. ≤ 2700 electrons r.m.s. for 1000 pF input capacitance, the shaping time being 7 μs. In the final version of the calorimeter the strips of each detector will be connected to the neighbouring one to form single strips 48 cm long. Two full-scale outputs are available and give, for an Si-D of 380 μm thickness, a linear response up to 25 or 400 mip, respectively. This range covers the very large dynamics required in the calorimeter. The readout is performed by means of a multiplexing system at a maximal frequency of 1 MHz.

An analog fast timing-out bipolar signal allows the auto-triggering based on the amount of the energy released in a given section of the calorimeter.

3. DATA TAKING

The prototype of the WiZard Si–W imaging calorimeter has been exposed to the PS Test Beam T7 at CERN, where a magnetic channel can select negative or positive charged particles of momentum between 1 and 8 GeV/c, $\Delta p/p = \pm 1\%$. The beam geometry and the arrangement of the counters are shown in fig. 4. The dimensions of the beam spot at the calorimeter entrance were defined by a circular counter S_2 of 1 cm diameter. The trigger was provided by the logical combinations $C_1{*}C_2{*}S_1{*}S_2{*}\overline{S}_3$ and $\overline{C}_1{*}\overline{C}_2\ S_1{*}S_2{*}\overline{S}_3$ of the S_i scintillation detectors and the C_i Cerenkov counters for the identification of electrons and pions respectively. Data have been collected in different runs at five beam energies between 1 and 8 GeV.

Data from the front-end electronics have been recorded by a standard acquisition system, allowing the storage of a complete event, and have been transferred via VME-bus to a microcomputer system (VALET-PLUS) for recording and on-line monitoring.

Dedicated pion calibration runs at 4 GeV were performed to establish the energy scale for each strip. The distance between the pedestal and the peak of the Landau distribution was taken as the energy unit (1 mip).

The calibration matrix has been measured strip by strip moving the prototype in the two transverse directions with respect to the beam by means of a remote-controlled mechanical support.

4. EXPERIMETNAL RESULTS AND SIMULATION

4.1 Energy response

The total energy contained in each single sampling layer or in the whole detector is found by adding the charge seen by all channels having an energy content above a threshold of 0.5 mip.

About 5% of the strips were damaged and their energy content was deduced from the adjacent strips.

We observed a capacitive coupling between the channels (2% – 3%), hence we used a correction based on the measured mean position of the pedestals during the runs with electrons.

The Monte Carlo simulation of the detector has been obtained with the Geant code version 3.14. In analogy with the data analysis procedure, the energy scale has been calibrated with 1 GeV pions. We chose the Landau–Vavilov–Gauss distribution to

simulate the fluctuations in the energy deposit. The cuts for the lowest energy were set for both photons and electrons at 50 keV.

The transverse and longitudinal energy containments for the prototype at these energies, as obtained from a MC calculation, can be deduced from table 3 where the respective percentage of containment is given.

Table 3

Monte Carlo calculated transverse and longitudinal containment of the prototype tower for sampling steps of 0.5 X_0

		Containment	
E_{inc} (GeV)	Longitudinal (% of E_{inc})	Transversal (% of E_{inc})	Total (% E_{inc})
1	96.0	63.9	60.0
2	93.2	65.8	59.0
4	89.7	67.7	57.4
6	87.6	68.5	56.2
8	86.1	69.4	55.5

The typical response of the strips to pions is given in fig. 5a, where the distribution of the mip energy loss is given in units of analog-to-digital converter (ADC) channels. From this figure it is also possible to evaluate a signal-to-noise ratio of better than 20, with an input capacitance of 80 pF. Figure 5b shows the distributions of detected energy for pions and electrons at 4 GeV whilst fig. 5c gives the distribution of the deposited energy for electrons at 2, 4, and 6 GeV.

The total charge released in the calorimeter by electrons at different energies (expressed in mip units) is given in fig. 6 together with data from MC simulation. The response of the calorimeter, in this energy range, shows a quasi-linear behaviour with deviations accounting for the partial containment at different energies (see Table 3).

Figure 7 a shows the relative energy resolution for the measured energies compared with MC simulation. Figure 7b shows the same data versus $1/\sqrt{E}$. The data are divided by the square root of the sampling step in units of radiation length $\sigma(E)/(E\sqrt{t})$, $t = 0.5\ X_0$. The two MC simulations also shown refer to sampling steps $t = 0.5\ X_0$ and $t = 1\ X_0$ this last indicates the potential performance of the calorimeter for full containment.

4.2 Shower shape and shower direction measurement

The total energy released by the electron shower is measured with a fine transverse and longitudinal segmentation. The longitudinal segmentation allows the identification of the position of the shower maximum along the axis of the shower. On the other hand, the two transverse coordinates of the shower axis can be derived from the centre of gravity of the x, y transverse energy distributions at each sampling plane.

Figure 8 shows the longitudinal development (experimental and simulated) of the showers initiated by 2 GeV electrons; the energy released is sampled over the 20 x, y sensitive planes.

Figure 9 shows simultaneously the longitudinal and the transverse energy distributions for 2 GeV electrons as seen from the y detectors only.

In fig. 10, the transverse shower profiles for 2, 4, 6 and GeV electrons are shown at the calorimeter depths of 2, 4, 6, and 8 X_0 for the horizontal strips.

From the centres of gravity of the transverse shower profiles measured at different depth in the calorimeter we have derived the direction of the incoming particle. This direction is given by the linear fit connecting the centres of gravity of the transverse shower profiles obtained for each sampling. The center of gravity position has been evaluated for each event and weighted by the square root of the deposited energy, as an error on this position the width of the transverse distribution mediated on all events has been taken.

The distribution of the slopes of these lines, for 4 GeV electrons, is shown for the x and y sampling in fig. 11a and b.

The mean value of these distributions confirms within the errors the normal incidence of the beam to the calorimeter entrance face. The σ value indicates the angular resolution of the imaging calorimeter. This σ is shown for the two views in figs. 12a and b as a function of the energy of the incoming electrons. As expected, the angular resolution improves with growing energy like the relative resolution in the energy measurement.

The same algorithm has been applied to the first four calorimeter planes. The angular spread of the particles directions so derived is represented in fig. 13 for 4 GeV electrons. Again assuming the normal incidence of the original particle, the σ value of the distribution of the slopes represents the capability for the first four calorimeter's planes of reconstructing the direction of the impinging particles. This is relevant for the application of similar structures as preshower detector.

For the aim of evaluating the capability of a single sampling plane of the calorimeter to identify the shower axis, we have taken as a reference the axis determined by all the sampling (excluding the one under analysis). The distribution of the differences between

the shower–axis reference position and the position obtained from one single sampling plane, indicates for that sampling plane the shower reconstruction capability . In Fig 14 a and b the widths of those distributions are reported as function of energy at two different depth in the calorimeter. Also in this case one notes the $1/\sqrt{E}$ behaviour of the position resolution.

4.3 Event pattern

The Si–W tracking calorimeter also reconstructs the event pattern, giving further information about the nature of the particle interaction. Some examples of event reconstruction for 2 GeV/*c* momentum particles are reported in figs. 14a,b and c, where the difference between the pattern of the shower induced by electrons and pions is clearly visible. By sampling the *x* and *y* shape of the shower development at each sensitive plane (0.5 X_0) the tracking calorimeter increases the power of discrimination between electrons and hadrons.

5. CONCLUSIONS

Tests on the tower prototype of the silicon tracking calorimeter have shown the capacity of this instrument to give detailed information on the shape of the shower development, combining the good resolution of the calorimeter and its high granularity. This allows identification of differently interacting particles, as required in the antimatter space research programme. The calorimeter can measure the direction of the photon-induced shower with an accuracy of a few millirad and can be used as a directional detector in the search for a point-like source in space for γ rays with energies of a few GeV.

The adequacy of the first part of this calorimeter as a pre-shower has also been proved experimentally.

Acknowledgements

We wish to thank L. Andreanelli and F. Bronzini, of the University `La Sapienza' of Rome, for their effort in producing a high-precision automatic mechanical support for the calorimeter. We also wish to thank the CERN PS machine staff and, in particular, the PS Coordinator R. Landua. Finally, our warm appreciation goes to K. Batzner for his help in the beam set-up.

References

[1] R.L. Golden et al., Nuovo Cimento **105B** (1990) 191 .

[2] M. Meschini et al., Nuovo Cimento **102B** (1988) 523.

[3] G. Barbiellini et al., Nucl. Instrum. Methods **A257** (1987) 543.

[4] P.G. Rancoita and A. Seidman, Nucl. Instrum. Methods **A263** (1988) 84.

[5] S. Pensotti et al., Nucl. Instrum. Methods **A265** (1988) 266.

[6] S. Pensotti et al., Nucl. Instrum. Methods **A270** (1988) 327.

[7] A.L.S. Angelis et al., preprint CERN–EP/90–73 (1990).

[8] To be published.

Figure captions

Fig. 1 Schematic view of the packaging of two detectors with perpendicular strips.

Fig. 2 a) Typical current voltage characteristics for a (3.6 × 58) mm^2 area strip (room temperature).

b) Typical capacity voltage curve, showing the onset of full depletion (room temperature).

Fig. 3 Pictorial view of the sequence of the sensitive Si–D's and the tungsten planes of the calorimeter inside the box.

Fig. 4 Schematic view of the beam set-up.

Fig. 5 a) Energy distribution for 4 GeV pions crossing a single Si–D.

b) Energy distribution for 4 GeV pions and electrons;

c) Energy distribution for 2, 4, and 6 GeV electrons.

Fig. 6 Energy response of the calorimeter, beam energy as a function of detected energy for electrons. The collected total mean charge is given in mip units versus the particle energy.

Fig. 7a Energy resolution compared with a MC simulation.

Fig. 7b Energy resolution data plotted against $1/\sqrt{E}$. The data are divided by the square root of the sampling step in units of radiation length, $\sigma(E)/(E\sqrt{t})$. The two MC simulations also reported refer to sampling steps $t = 0.5\ X_0$ and $t = 1\ X_0$; this last shows the potential performance of the calorimeter for full containment.

Fig. 8 Longitudinal development (experimental and simulated) of a 2 GeV electron shower. The energy is sampled in 20 sensitive planes.

Fig. 9 Three-dimensional plot of the longitudinal and transverse energy distributions for 2 GeV electrons.

Fig. 10 Transverse shower profiles for electrons 2 GeV (dotted lines), 4 GeV (dashed lines) and 6 GeV (solid lines). The profiles are analyzed at the calorimeter depths of: a) 2 X_0, b) 4 X_0, c) 6 X_0, d) 8 X_0.

Fig. 11 Distribution of the slopes of the measured directions of the particles, for incoming electrons at 4 GeV: a) for x sampling and b) for y sampling. The σ value of these distributions indicates the angular resolution.

Fig. 12 The angular resolution of the imaging calorimeter is shown for the two views x and y as a function of the energy of the incoming electrons, the line corresponds to a $1/\sqrt{E}$ fit.

Fig. 13 Angular spread of the 4 GeV electrons shower axis as derived from the centres of gravity of the transverse shower profile in the first four contiguous sampling planes.

Fig. 14 Widths of the distributions of the differences between the shower–axis reference position and the position obtained from one single sampling plane reported as function of energy at two different depth in the calorimeter, 14 a after 2 X_0 and b after 4 X_0.

Fig. 15 Examples of pattern reconstruction for 2 GeV/*c* particles:
a) interacting pion; b) electromagnetic shower c) non-interacting pion. The dimensions of the squares represents the amount of energy released in each stripe.

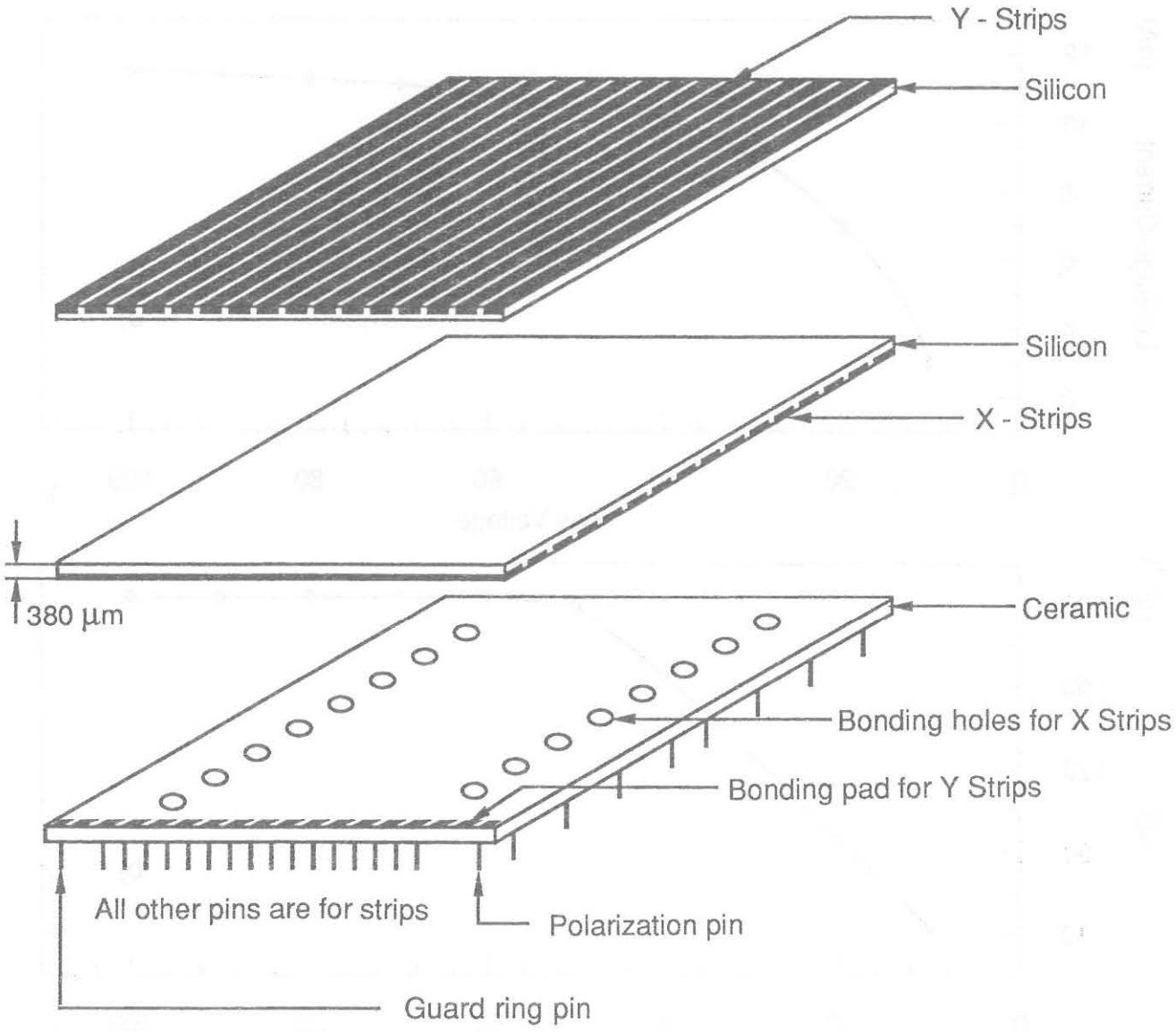
Y - Strips
Silicon
Silicon
X - Strips
380 µm
Ceramic
Bonding holes for X Strips
Bonding pad for Y Strips
All other pins are for strips
Polarization pin
Guard ring pin

Fig. 1

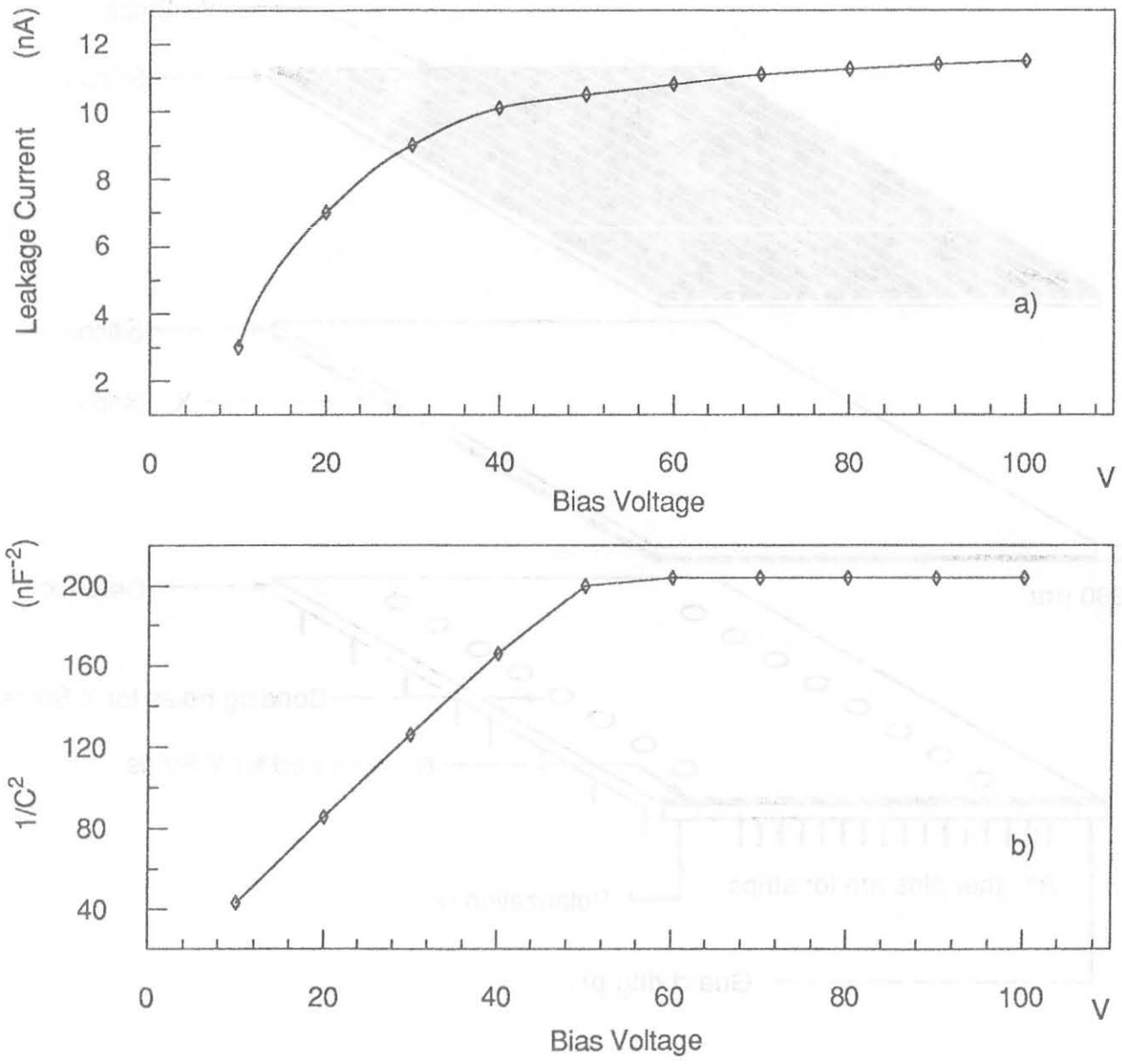
Leakage Current (nA)
12
10
8
6
4
2
0
20
40
60
80
100
V
Bias Voltage
a)
1/C² (nF⁻²)
200
160
120
80
40
0
20
40
60
80
100
V
Bias Voltage
b)

Fig. 2

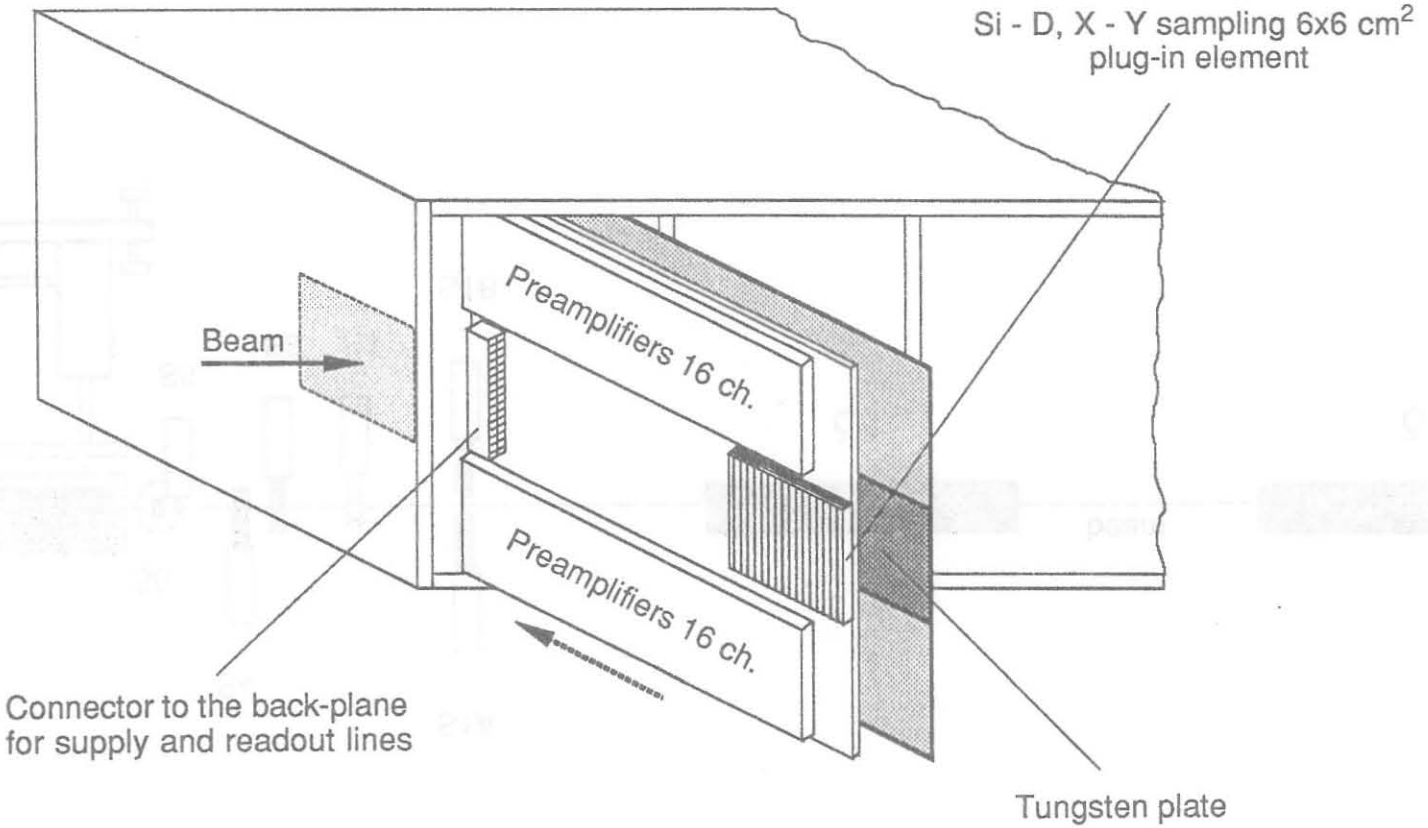
Si - D, X - Y sampling 6x6 cm^2
plug-in element
Beam
Preamplifiers 16 ch.
Preamplifiers 16 ch.
Connector to the back-plane
for supply and readout lines
Tungsten plate

Fig. 3

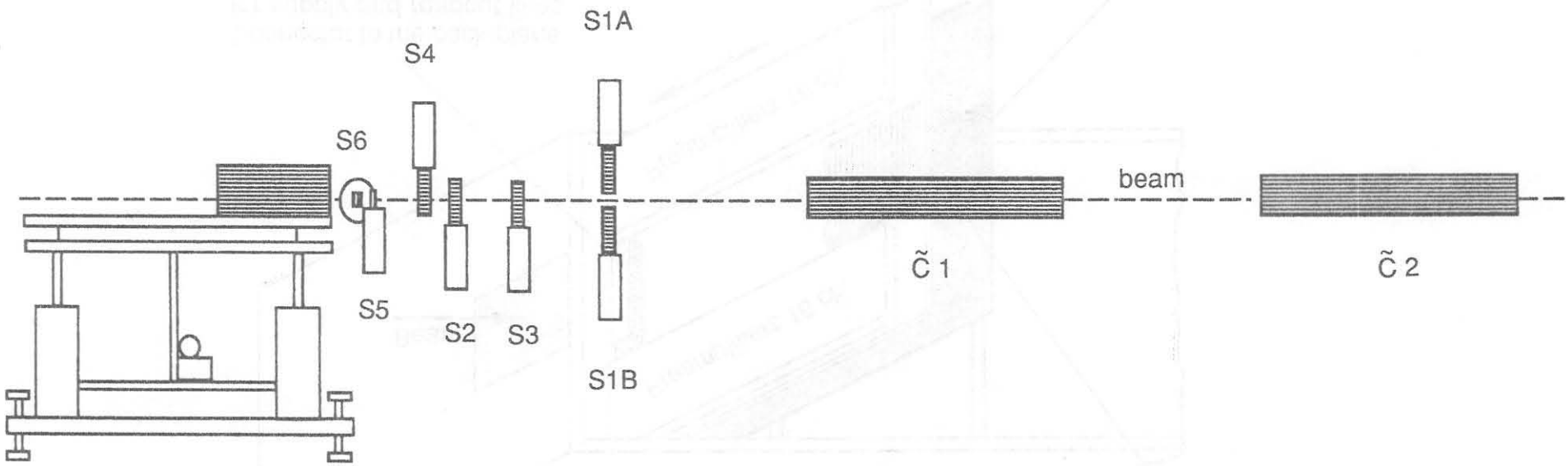

Fig. 4

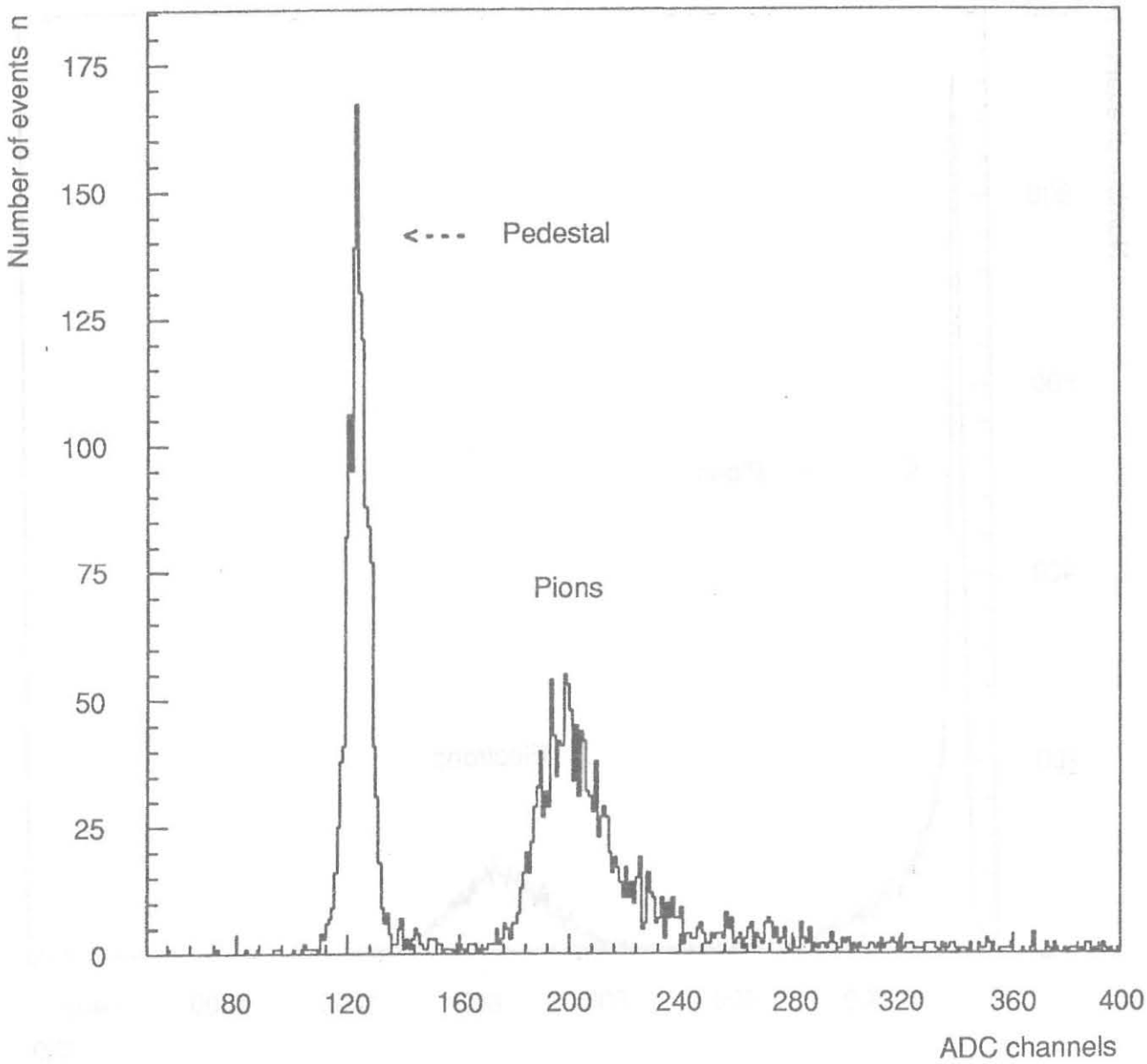
Number of events n
175
150
125
100
75
50
25
0
<--- Pedestal
Pions
80
120
160
200
240
280
320
360
400
ADC channels

Fig. 5a

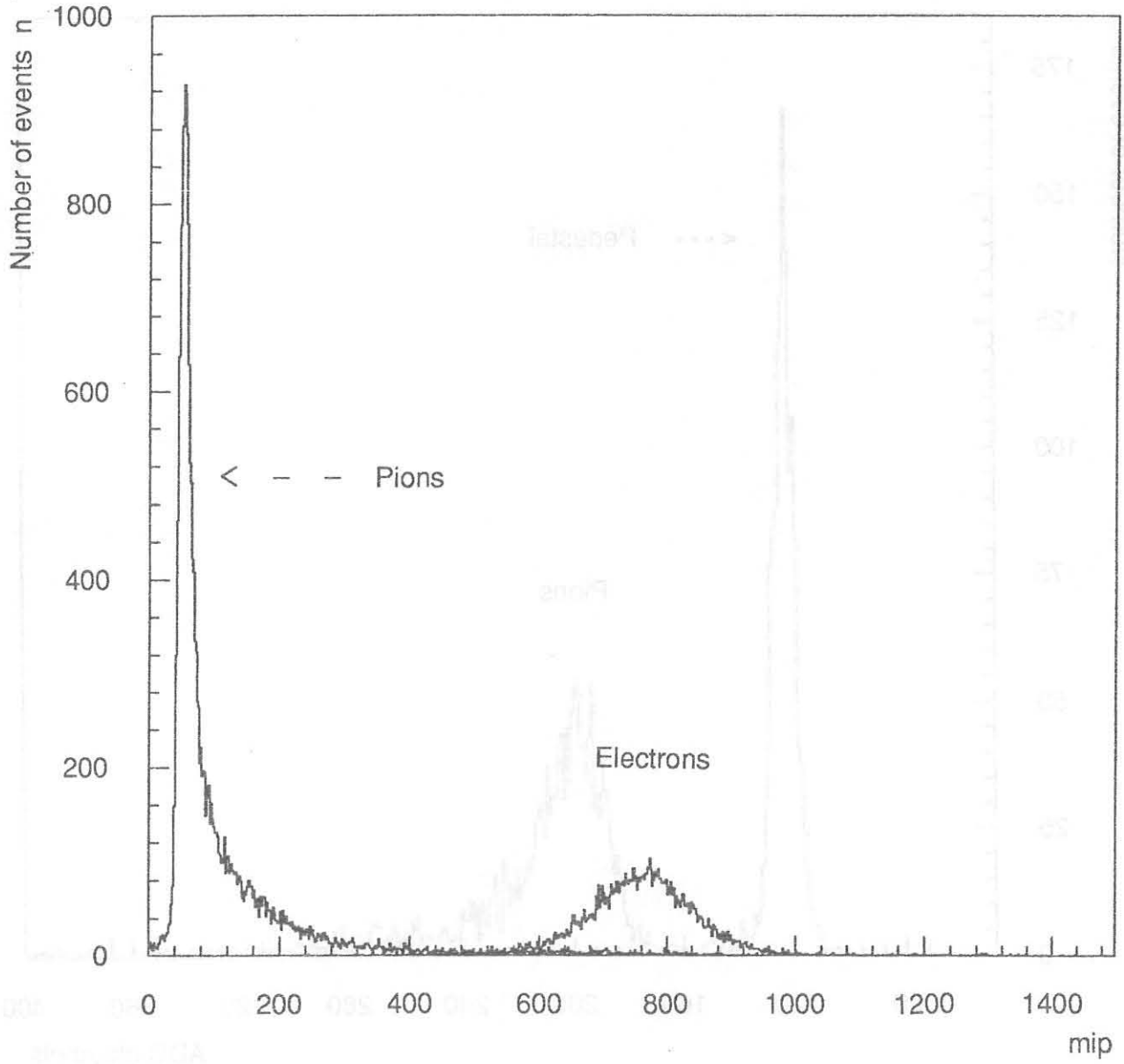
Number of events n
1000
800
600
400
200
0
< – – Pions
Electrons
0
200
400
600
800
1000
1200
1400
mip

Fig. 5b

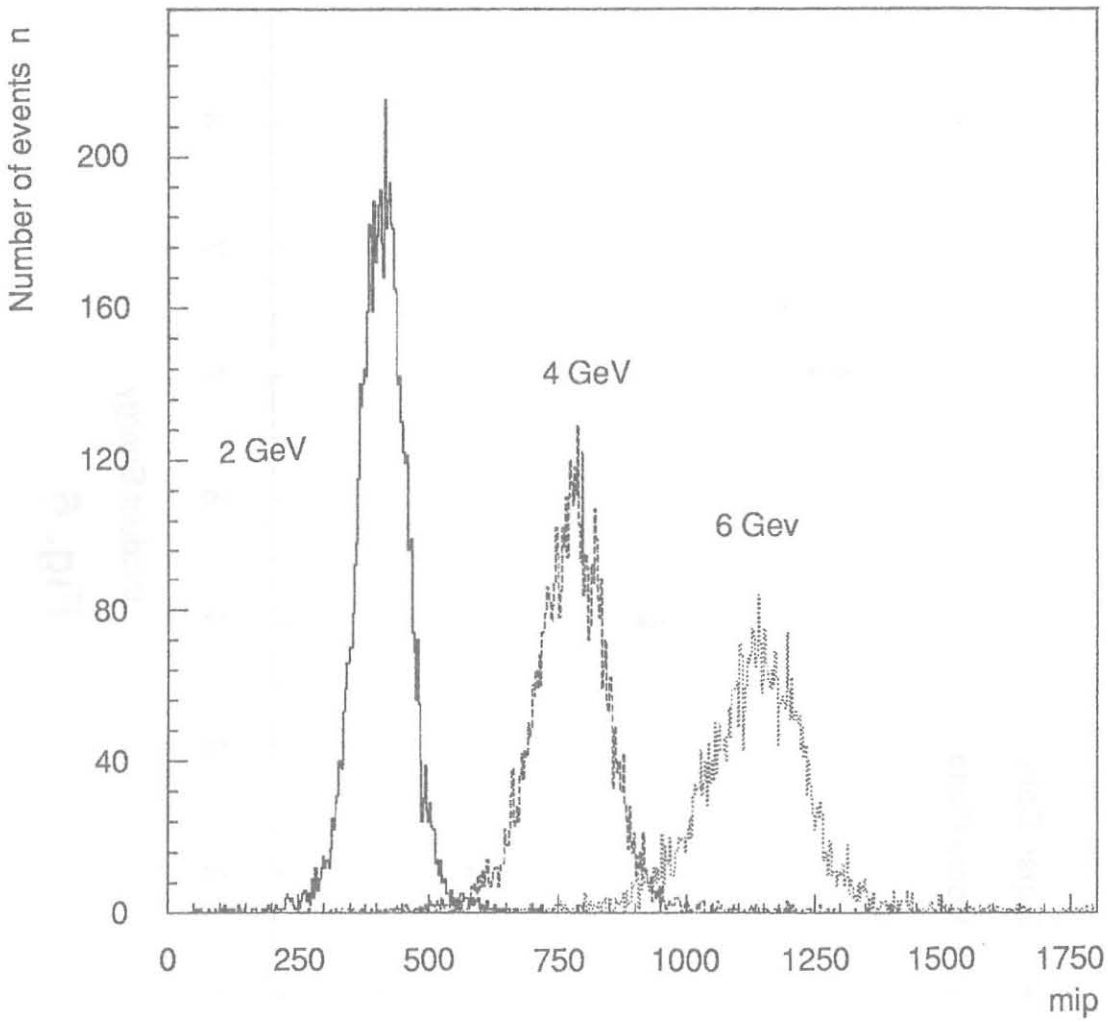
Number of events n
200
160
120
80
40
0
2 GeV
4 GeV
6 Gev
0
250
500
750
1000
1250
1500
1750
mip

Fig. 5c

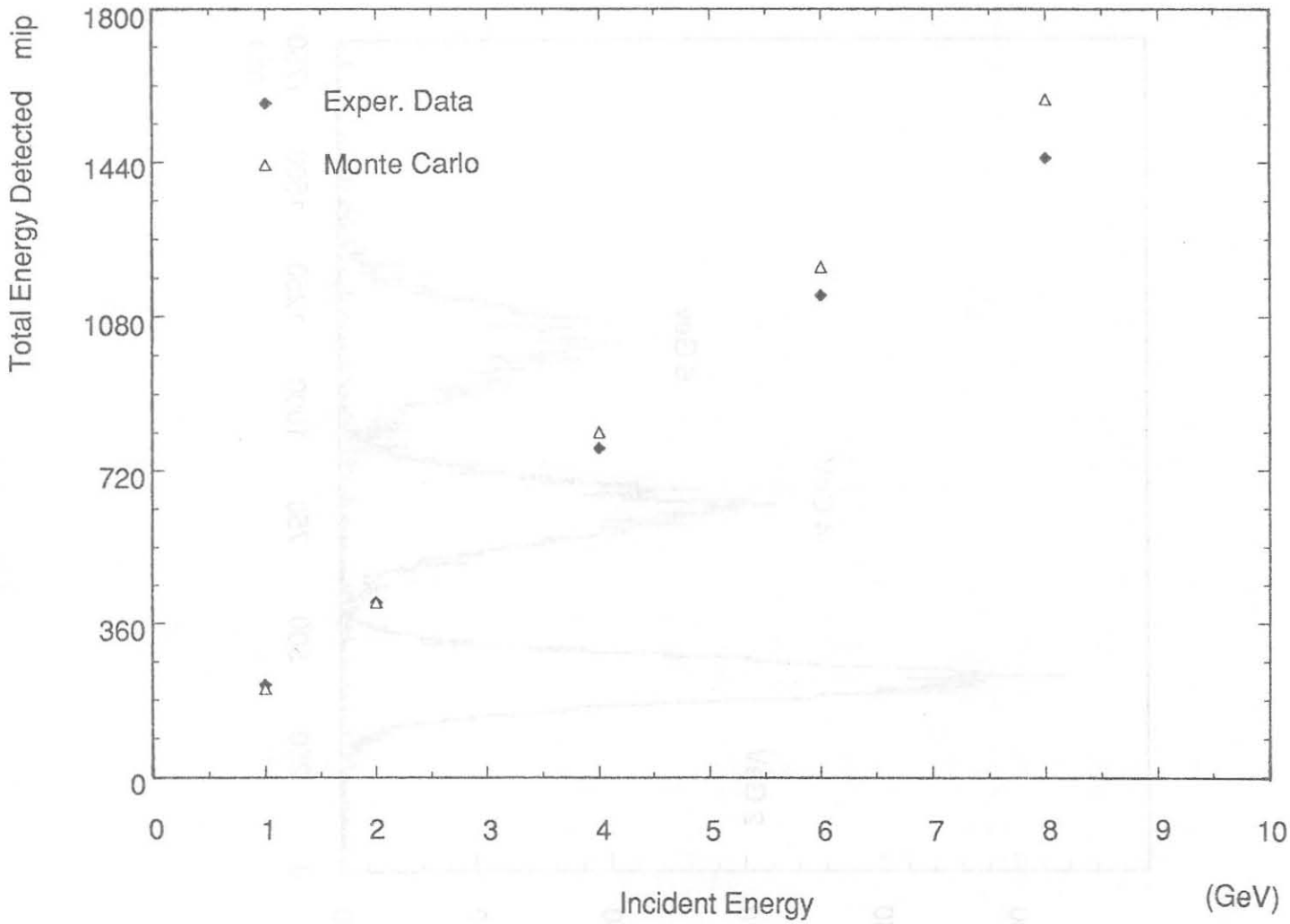
Total Energy Detected mip
1800
1440
1080
720
360
0
Exper. Data
Monte Carlo
0
1
2
3
4
5
6
7
8
9
10
Incident Energy
(GeV)

Fig. 6

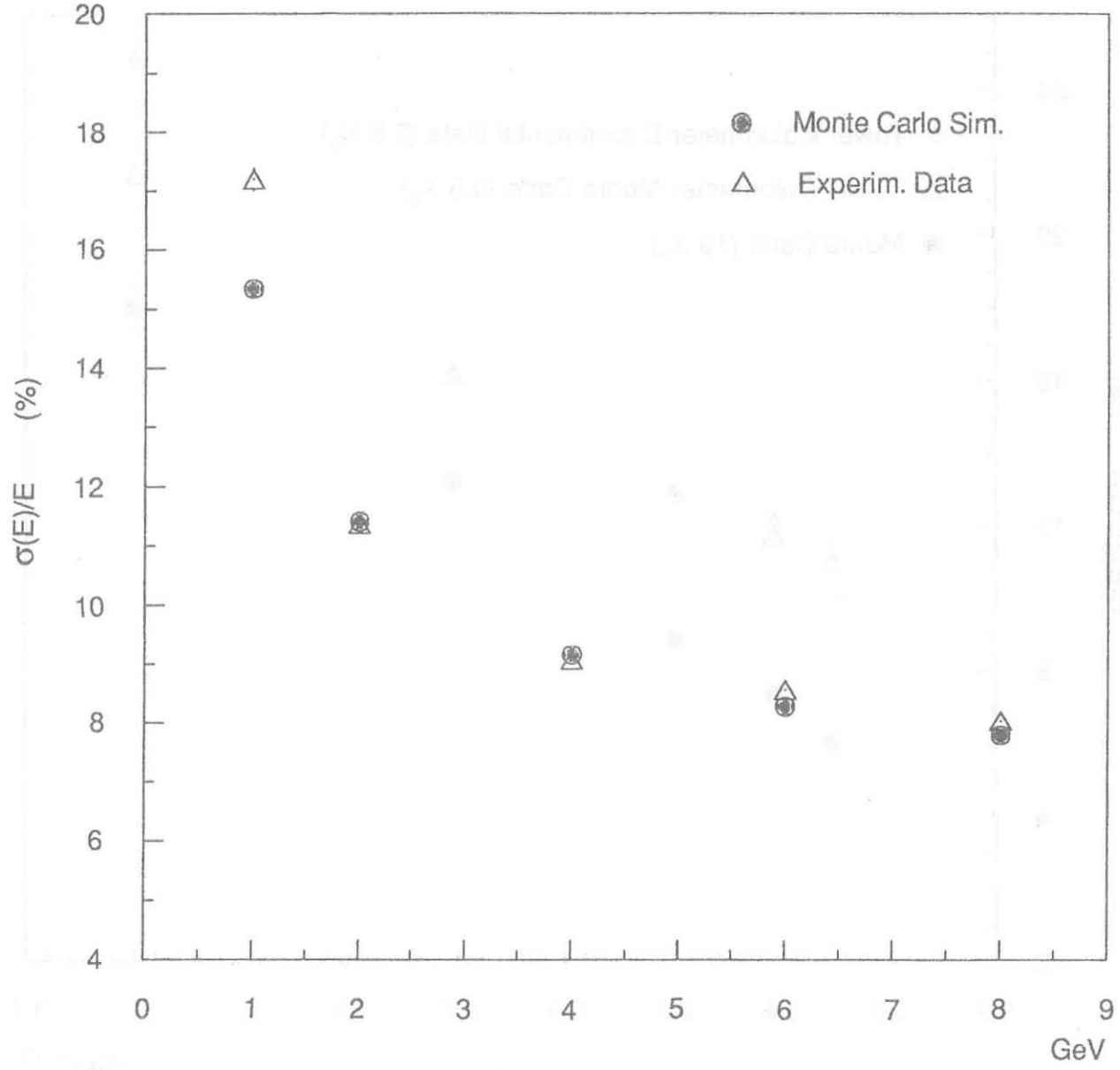
20
18
16
14
12
10
8
6
4
σ(E)/E (%)
Monte Carlo Sim.
Experim. Data
0
1
2
3
4
5
6
7
8
9
GeV

Fig. 7a

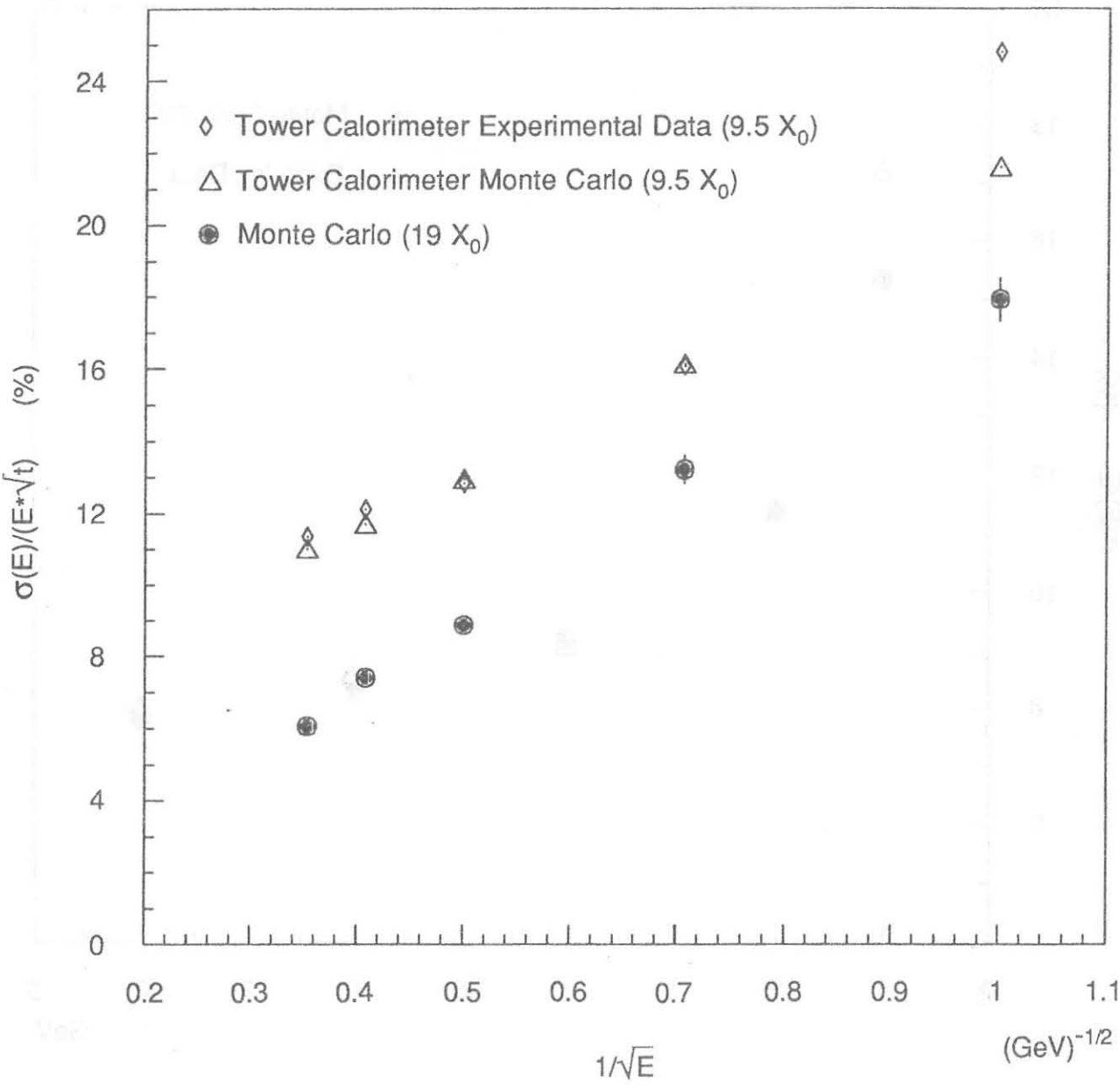
◊ Tower Calorimeter Experimental Data (9.5 X_0)
△ Tower Calorimeter Monte Carlo (9.5 X_0)
● Monte Carlo (19 X_0)
σ(E)/(E*√t) (%)
24
20
16
12
8
4
0
0.2
0.3
0.4
0.5
0.6
0.7
0.8
0.9
1
1.1
1/√E
(GeV)$^{-1/2}$

Fig. 7b

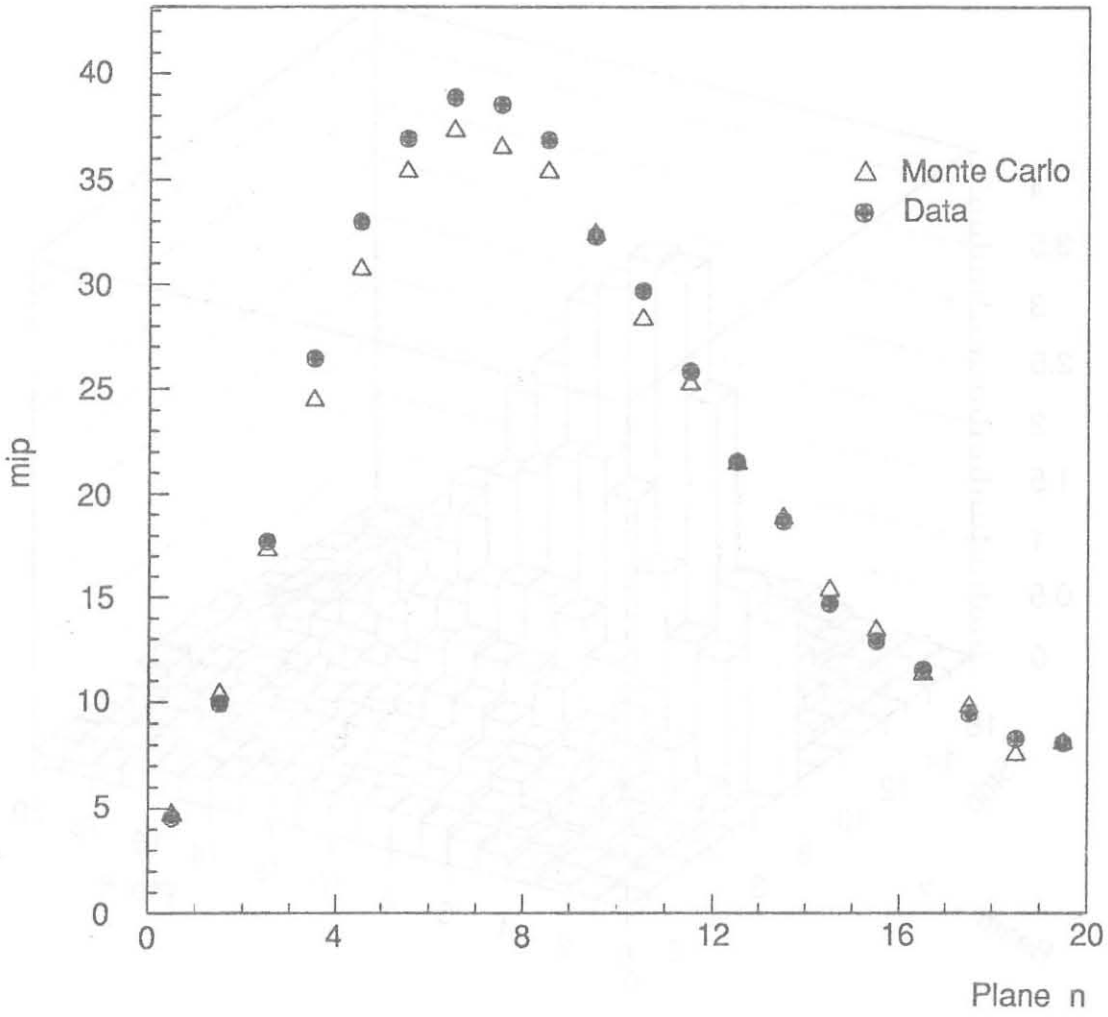

Fig. 8

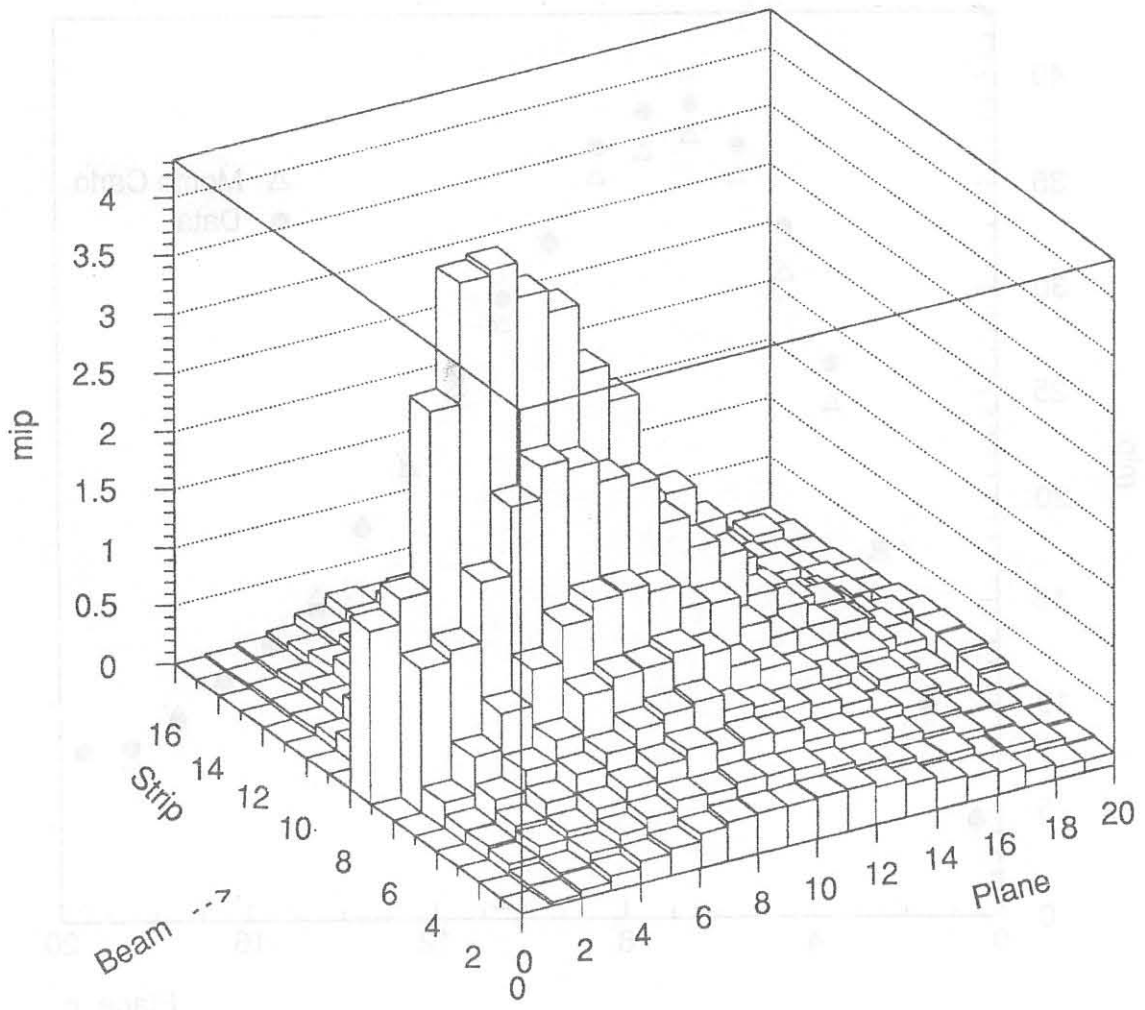
mip
4
3.5
3
2.5
2
1.5
1
0.5
0
Strip
16
14
12
10
8
6
4
2
0
Beam
0
2
4
6
8
10
12
14
16
18
20
Plane

Fig. 9

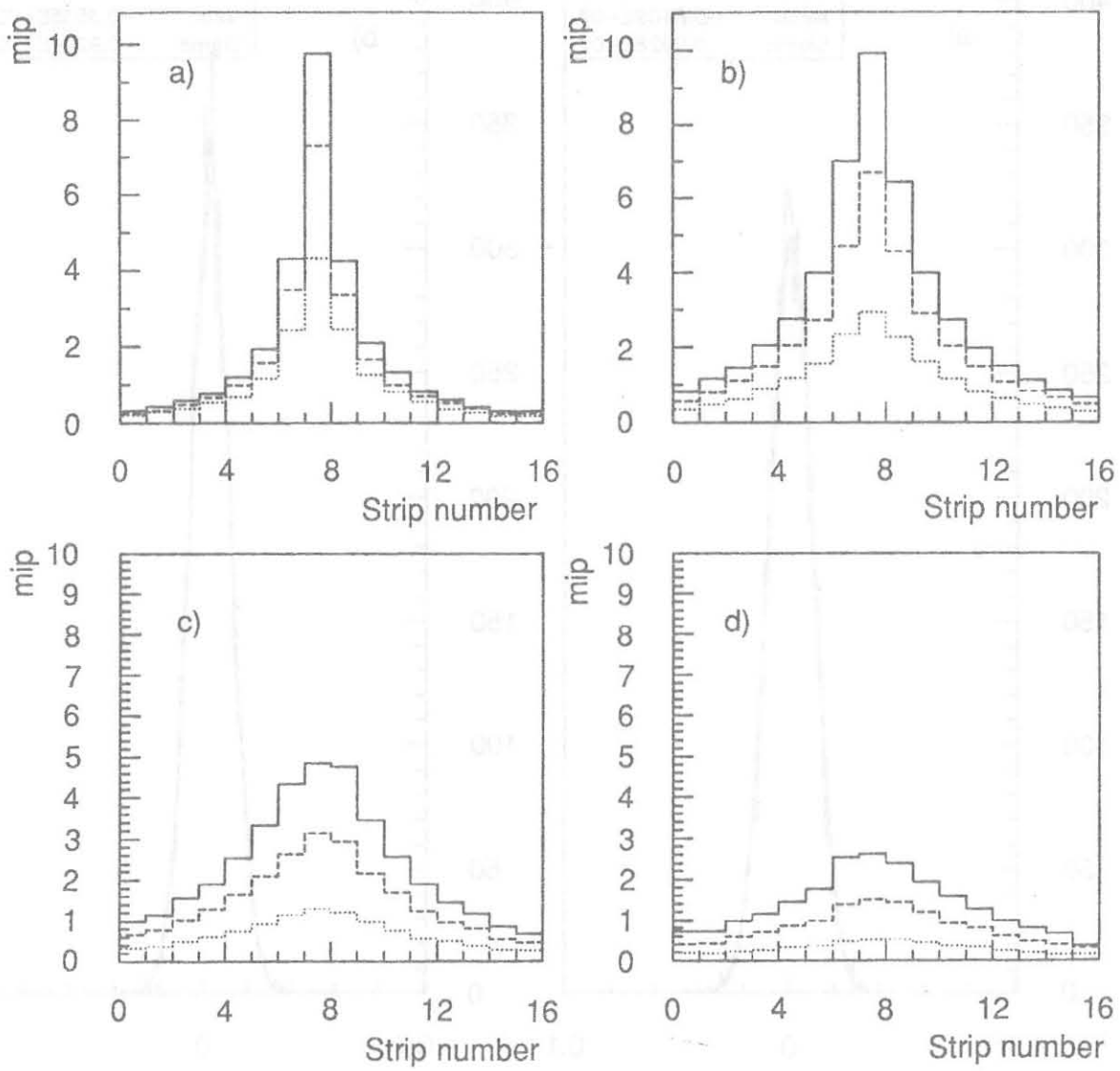

Fig. 10

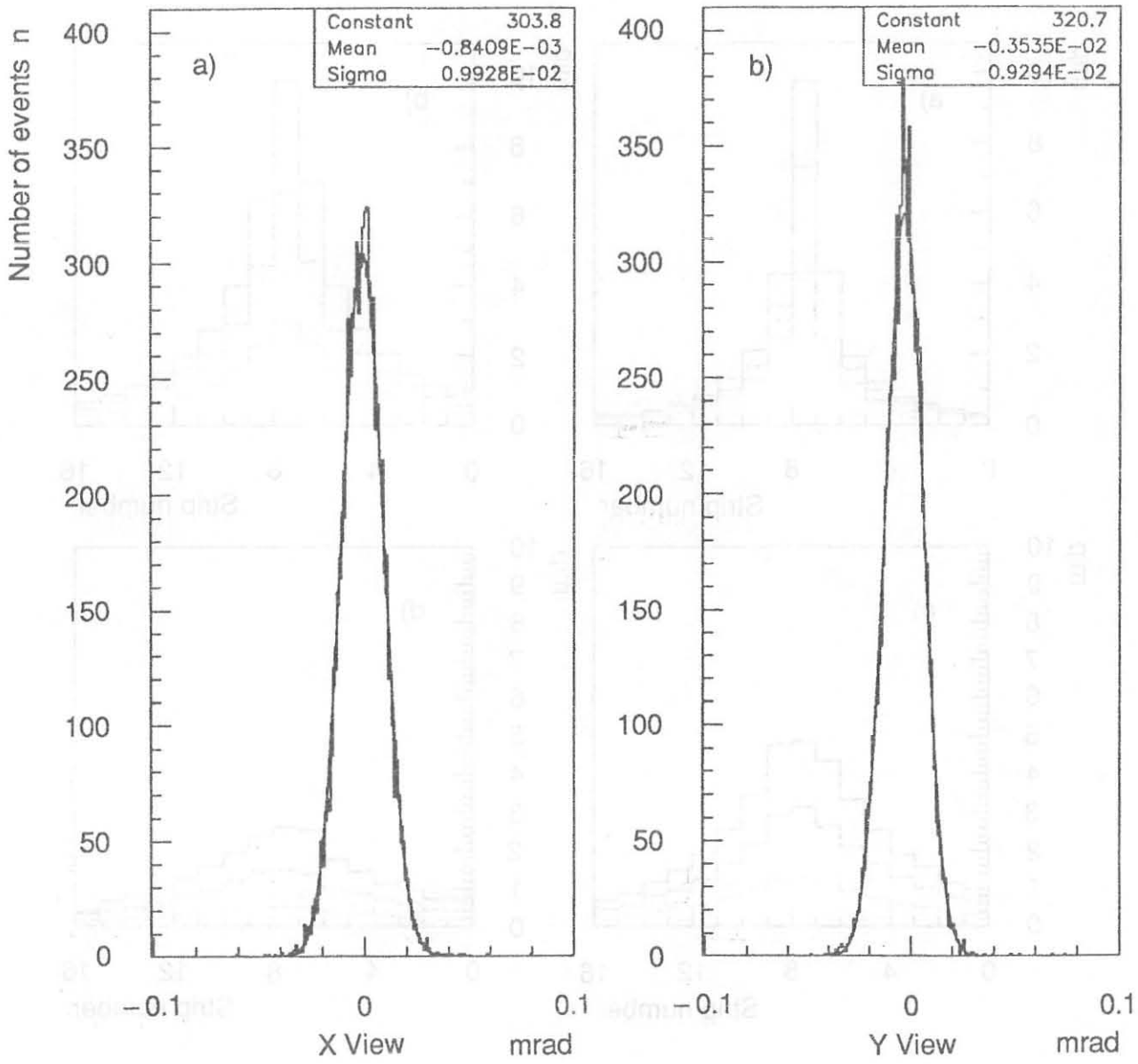
Number of events n
400
350
300
250
200
150
100
50
0
a)
Constant 303.8
Mean −0.8409E−03
Sigma 0.9928E−02
−0.1
0
0.1
X View
mrad
b)
Constant 320.7
Mean −0.3535E−02
Sigma 0.9294E−02
Y View
mrad

Fig. 11

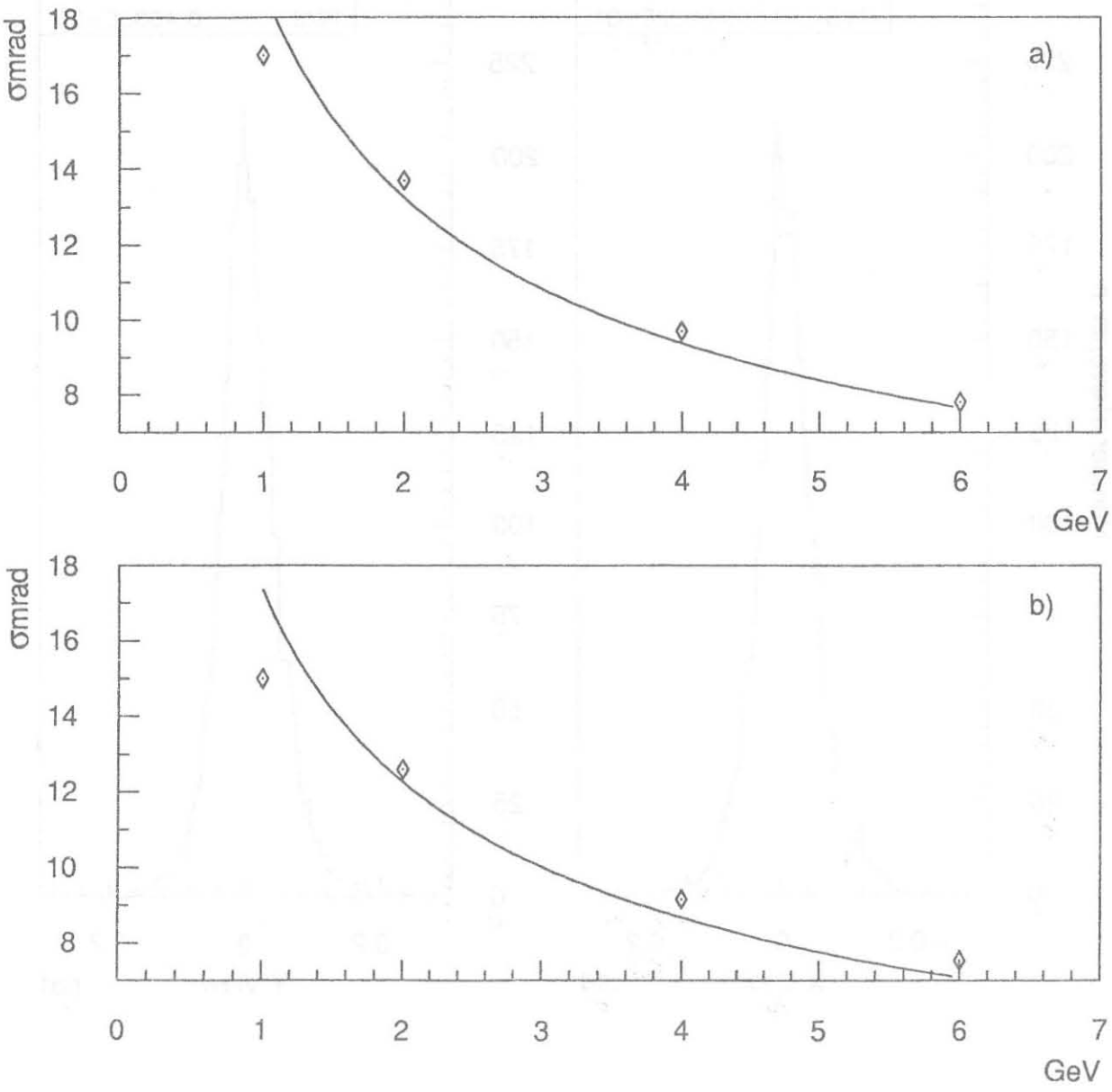
σmrad
18
16
14
12
10
8
a)
0
1
2
3
4
5
6
7
GeV
σmrad
18
16
14
12
10
8
b)
0
1
2
3
4
5
6
7
GeV

Fig. 12

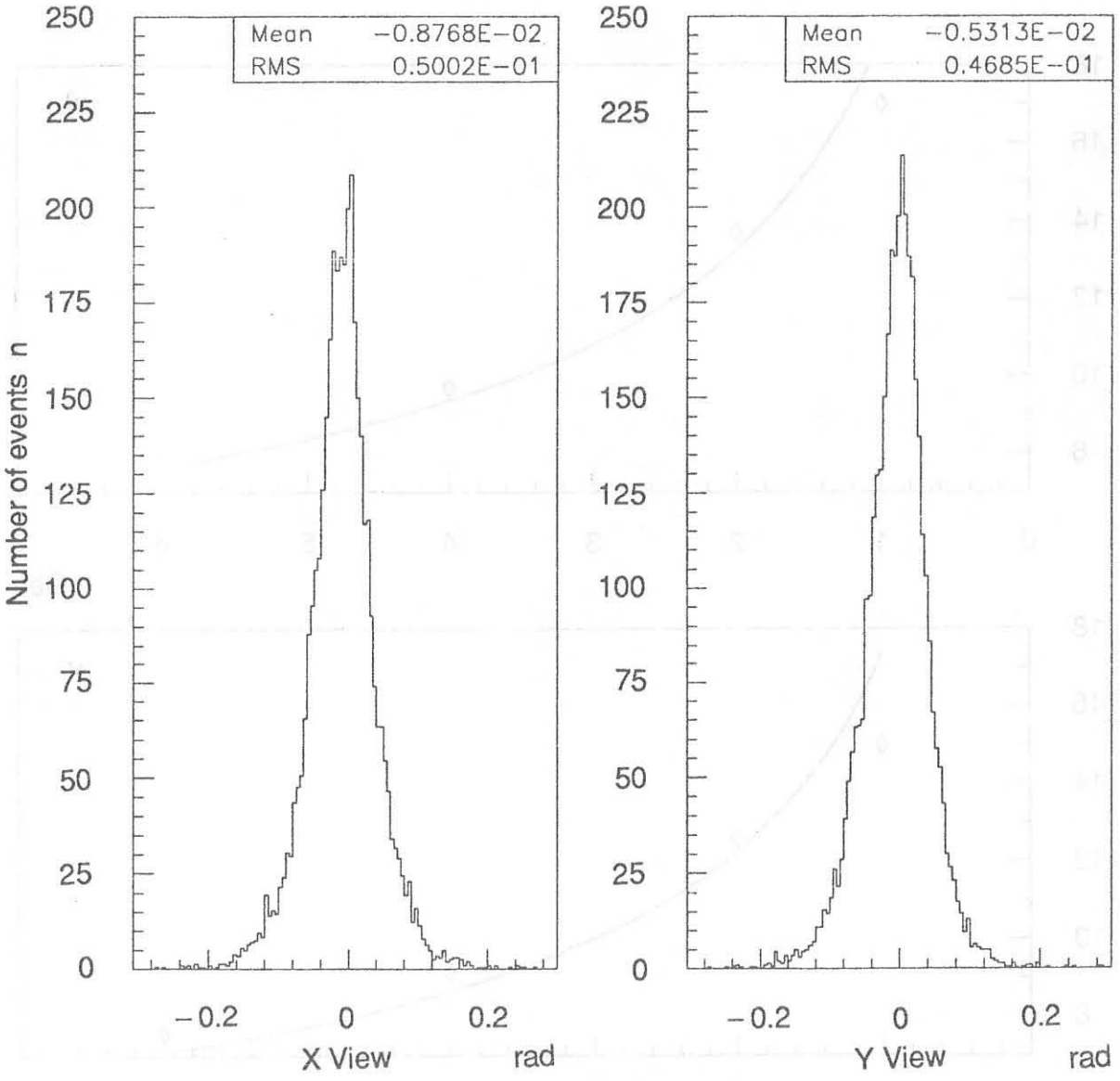
Mean −0.8768E−02
RMS 0.5002E−01
Number of events n
250
225
200
175
150
125
100
75
50
25
0
−0.2
0
0.2
X View
rad
Mean −0.5313E−02
RMS 0.4685E−01
Y View
rad

Fig. 13

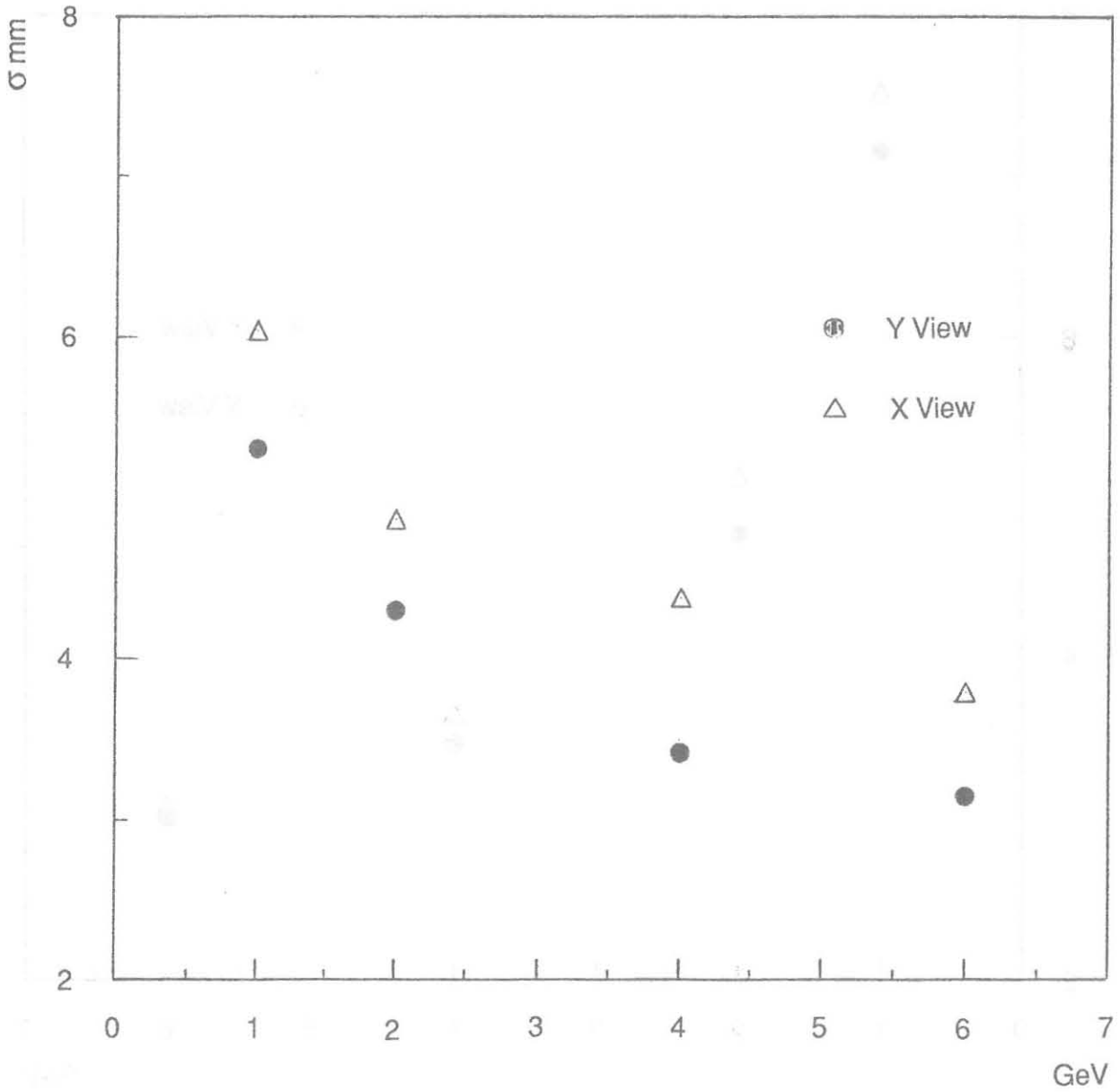

Fig. 14a

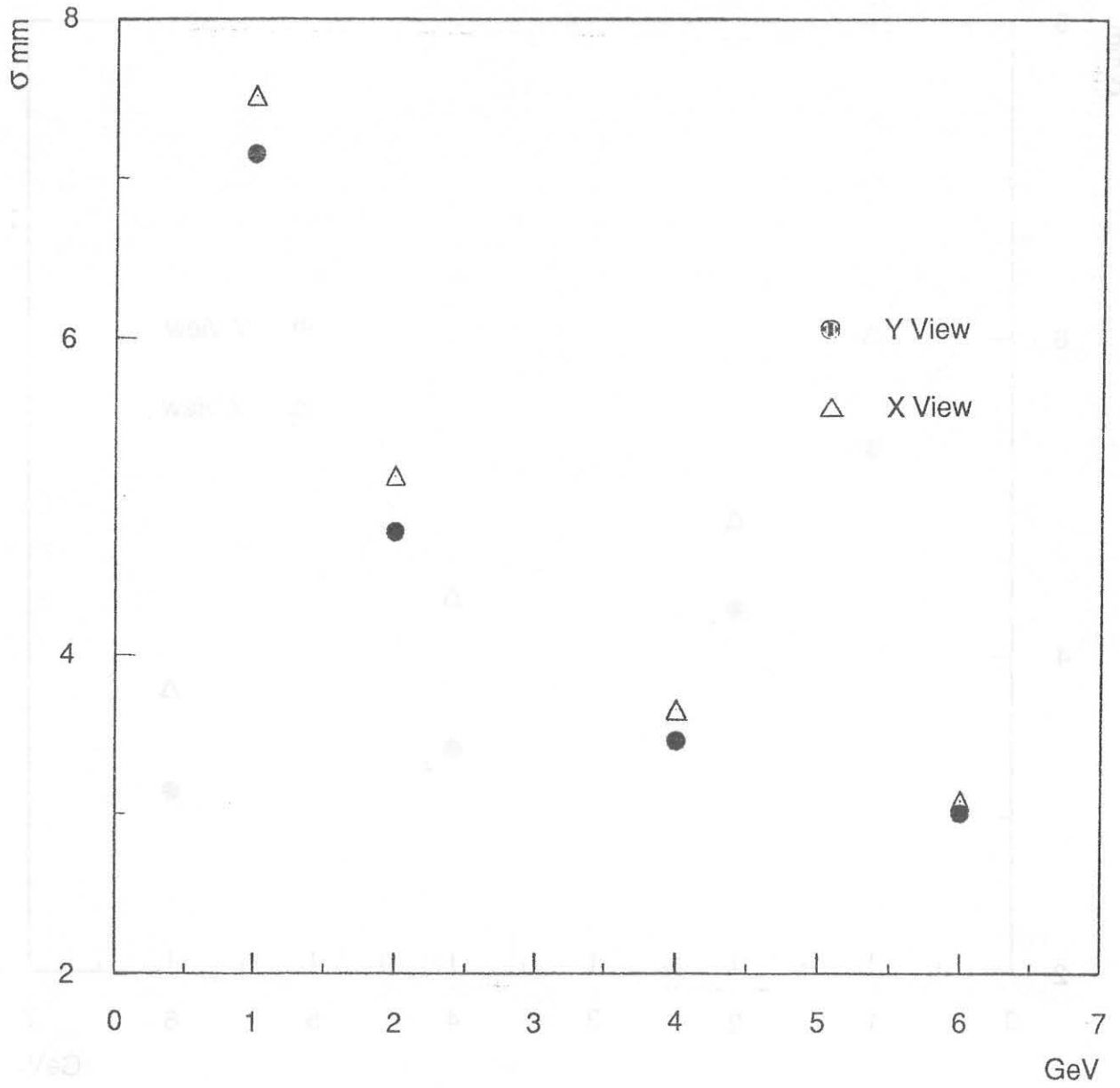

Fig. 14b

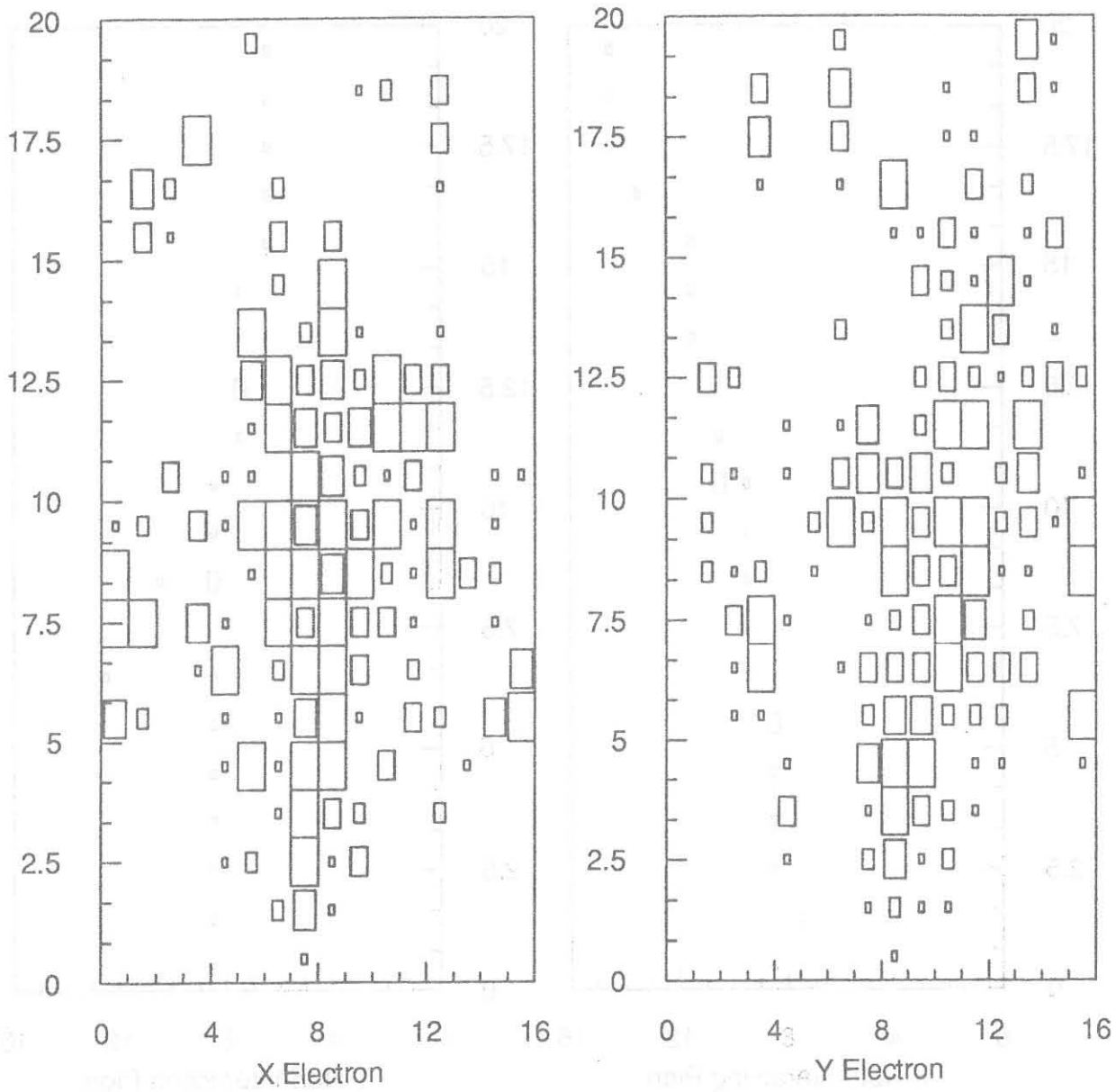
20
17.5
15
12.5
10
7.5
5
2.5
0
0
4
8
12
16
X Electron
20
17.5
15
12.5
10
7.5
5
2.5
0
0
4
8
12
16
Y Electron

Fig. 15a

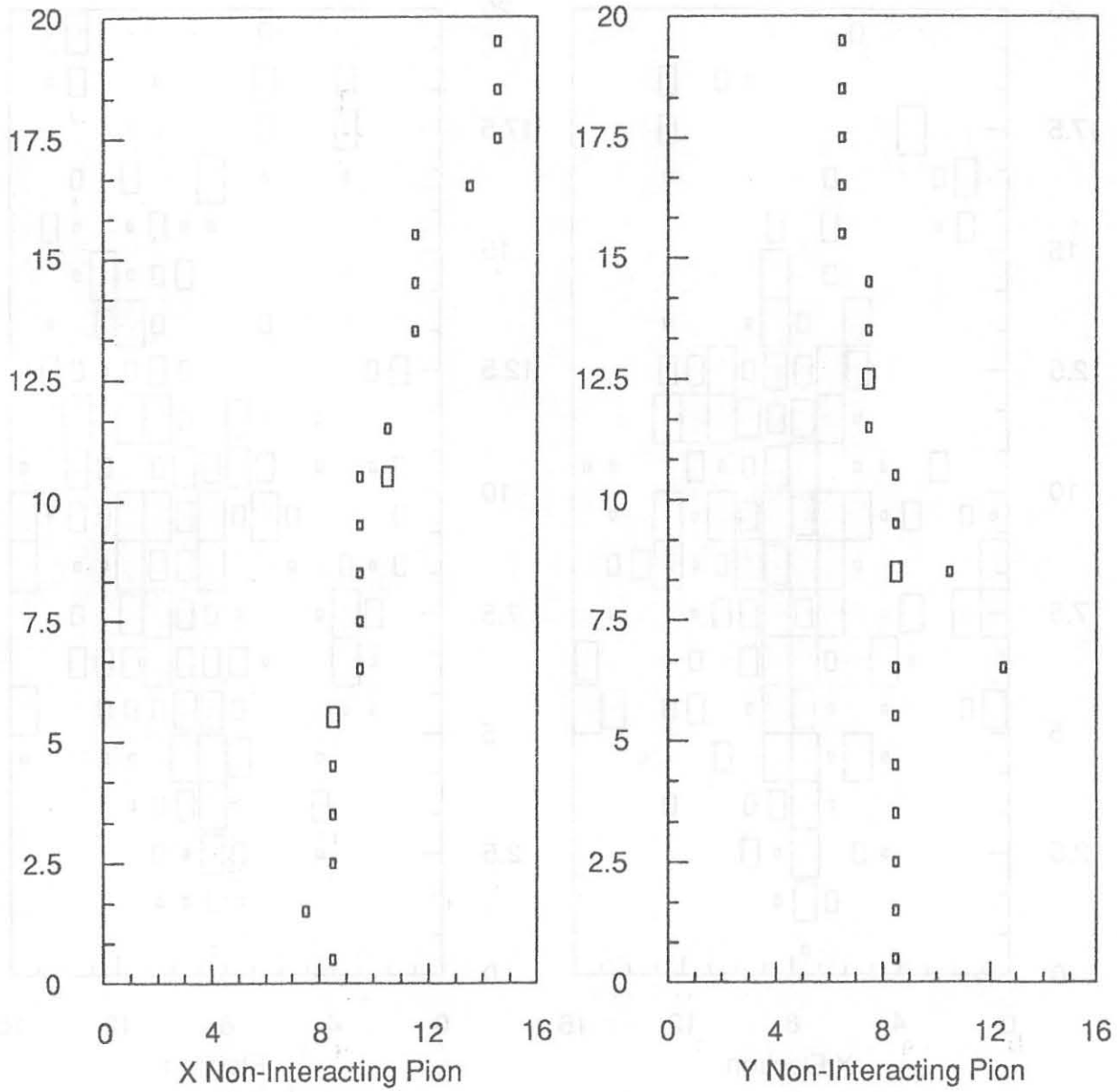
20
17.5
15
12.5
10
7.5
5
2.5
0
0
4
8
12
16
X Non-Interacting Pion
20
17.5
15
12.5
10
7.5
5
2.5
0
0
4
8
12
16
Y Non-Interacting Pion

Fig. 15b

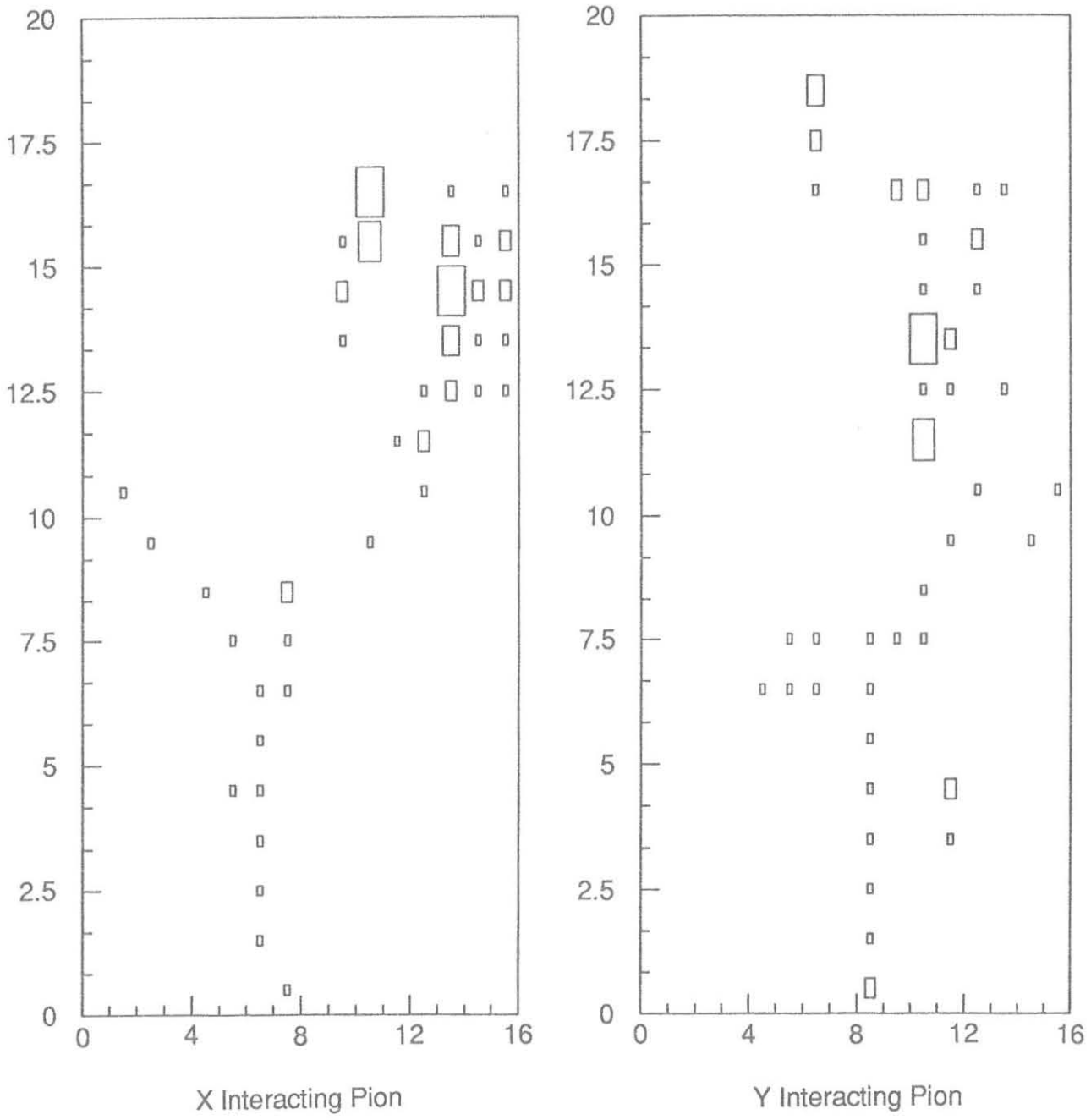
20
17.5
15
12.5
10
7.5
5
2.5
0
0
4
8
12
16
X Interacting Pion
Y Interacting Pion

Fig. 15c